The commotion project

Computational methods for moving and deforming objects in extreme waves

Veldman, Arthur E.P.; van der Plas, Peter; Seubers, Henk; Hosseini Zahraei, S.M.; Chang, X.; Wellens, P.R.; Helder, Joop

**Publication date**
2019

**Document Version**
Final published version

**Published in**
8th International Conference on Computational Methods in Marine Engineering, MARINE 2019

**Important note**
To cite this publication, please use the final published version (if applicable).
Please check the document version above.

# THE COMMOTION PROJECT: COMPUTATIONAL METHODS FOR MOVING AND DEFORMING OBJECTS IN EXTREME WAVES

## ARTHUR E.P. VELDMAN[1*], PETER VAN DER PLAS[1,3], HENK SEUBERS[1], S. MATIN HOSSEINI ZAHRAEI[2], XING CHANG[2], PETER R. WELLENS[2] AND JOOP HELDER[3]

[1] Bernoulli Institute for Mathematics, Computer Science and Artificial Intelligence,
University of Groningen, PO Box 407, 9700AK Groningen, The Netherlands
e-mail: {a.e.p.veldman, h.seubers}@rug.nl

[2] Department of Maritime and Transportation Technology, Delft University of Technology,
Mekelweg 2, 2628 CD Delft, The Netherlands
e-mail: {s.hosseinizahraei, x.chang, p.r.wellens}@tudelft.nl

[3] MARIN, PO Box 28, 6700AA Wageningen, The Netherlands
e-mail: {p.v.d.plas, j.helder}@marin.nl

**Key words:** Extreme waves, fluid–solid body interaction, CFD, local grid refinement, experimental validation.

**Abstract.** Extreme waves and their impact on (fixed and floating) offshore structures have long been subjects that could only be studied with experimental methods; sufficiently accurate existing numerical methods (CFD) are only recently emerging. Phenomena like green water loading and slamming are highly dependent on the relative motion of a ship versus the oncoming wave crests, as influenced by the preceding wave groups. Thus, accurate prediction of the hydrodynamic forces requires methods that can reliably predict the interaction between extreme waves and body dynamics. Over the years, the ComFLOW simulation method has been developed to cover this CFD niche. A novel ingredient devceloped in the ComMotion project is an unsteady coupling algorithm that is numerically stable under all circumstances (such as ratio of body mass versus added mass). Also, a new class of absorbing boundary conditions has been extended to include the effects of current. Several applications will be presented, including esperimental validation.

## 1 INTRODUCTION

Under extreme weather conditions, waves and currents can induce large forces and stresses on sea-going ships and offshore constructions (production and offloading platforms, mooring systems, wind turbine farms) [1]. For example, in heavy storms solid amounts of seawater,

1

called 'green water', flow over the deck, thus threatening the safety and operability of the ship. The amount of shipped water obviously depends on the phase between ship and wave motion, and hence on the preceeding wave group and its interaction with the ship dynamics. The same holds for slamming impacts against a ship's bow. As a special case, free fall lifeboats (Fig. 1) face these challenges when a ship or platform needs to be evacuated.
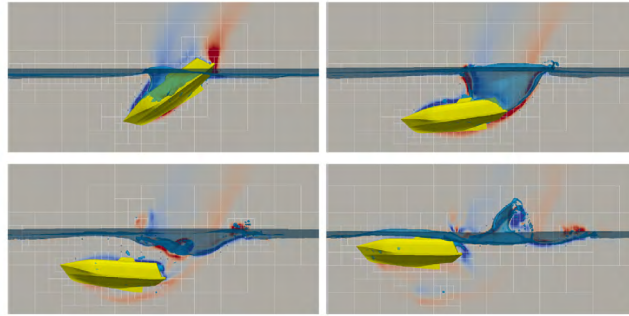


**Figure 1**: Simulated snapshots of a free-fall life boat.

Until recently, these violent flow phenomena were mainly studied experimentally, but there is a growing need for a numerical simulation tool capable of predicting in detail the hydrodynamic loads due to slamming and green water; see, e.g., [2–4]. However, the tools currently available are based on e.g. linear potential flow theory or shallow-water theory; see e.g. [5]. These tools based on simple models are hardly capable of predicting such events to an acceptable level of accuracy. The physical phenomena accompanying extreme events are both highly non-linear and highly dispersive due to the occurring wave steepness, and require new methods as a basis for the prediction of the water flow and its induced hydrodynamic loads.

It is only recently that the Navier–Stokes equations can be solved for large-scale complex free-surface flow problems, thanks to novel numerical algorithms and the increase in computer power [6–8]. For an overview of basic Navier–Stokes methods for free-surface flow we refer to [9], with some offshore applications in [10–12].

In this paper we will present the main physical and numerical ingredients of the ComMotion project:

  – Interactively moving bodies.
  – Hydroelasticity.
  – Absorbing boundary conditions incorporating current.
  – Experimental validation.

For reliable load predictions in these examples, it is necessary to determine the position and dynamics of the objects as part of the flow simulation. The ComMotion project makes this major step by extending the ComFLOW simulation method to interactively moving and deforming objects in extreme waves. Also, attention is paid to numerical absorbing outflow boundary conditions in the presence of current. The new developments will be illustrated with a number of maritime applications.

2

## 2 MODELLING

### 2.1 Flow model

Incompressible, turbulent fluid flow can be modelled by means of the Navier–Stokes equations.

$$M\mathbf{u} = 0, \qquad \frac{\partial \mathbf{u}}{\partial t} + C(\mathbf{u})\mathbf{u} + Gp - V\mathbf{u} = \mathbf{f}. \tag{1}$$

The divergence operator is denoted $M \equiv \nabla\cdot$, the convection operator $C(\mathbf{u})\mathbf{v} \equiv \nabla \cdot (\mathbf{u} \otimes \mathbf{v})$, the pressure gradient operator $G = \nabla$, the viscous diffusion operator $V(\mathbf{u}) \equiv \nabla\cdot\nu\nabla\mathbf{u}$ and $\mathbf{f}$ a forcing term. The kinematic viscosity is denoted by $\nu$. Turbulence is modelled by means of large-eddy simulation (LES) using a state-of-the-art low-dissipation QR/AMD-model [13–16]. For its use in maritime applications, see [17, 18].

The evolution of the free water surface is described by an adapted and improved version of the Volume-of-Fluid method (VOF) introduced in [6] and [19]. The free surface is reconstructed by Youngs' PLIC method [20, 21] and advanced by a local height function [21, 22]. Specifically, use will be made of the ComFLOW simulation method, developed at the University of Groningen in cooperation with the Technical University of Delft and MARIN. It is described in full detail in a handful of PhD theses [18, 21–27].

Bodies can move and deform through the fixed Cartesian grid, with their position described in a cut-cell fashion by edge and volume apertures, as is done for non-moving objects [28] (see also [29, 30]). Local grid refinement [31] can be applied in 'interesting' regions.

The Navier–Stokes equations (1) are discretized on a staggered computational grid [32]. The second-order finite-volume discretization of the continuity equation at the 'new' time level $\cdot^{n+1}$ is given by

$$\mathsf{M}_0\mathbf{u}^{n+1} = -\mathsf{M}_\Gamma\mathbf{u}_\Gamma^{n+1}, \tag{2}$$

where $\mathsf{M}_0$ acts on the interior of the domain and $\mathsf{M}_\Gamma$ acts on the boundaries. The discretization keeps convection $\mathsf{C}(\mathbf{u}_h)$ skew symmetruc and diffusion $\mathsf{V}$ symmetric. In this exposition, for simplicity reasons the first-order forward Euler time integration will be used. In the actual calculations, a second-order Adams–Bashforth method for convection and a fully implicit method for diffusion is applied.

The discrete momentum equation can be formulated as

$$\mathbf{u}^{n+1} = \tilde{\mathbf{u}} - \delta t\,\Omega^{-1}\mathsf{G}\mathsf{p}^{n+1}, \quad \text{where} \quad \tilde{\mathbf{u}} = \mathbf{u}^n + \delta t\,\Omega^{-1}[-\mathsf{C}(\mathbf{u}^n)\,\mathbf{u}^n + \mathsf{V}\mathbf{u}^n + \mathbf{f}]. \tag{3}$$

Here, the diagonal matrix $\Omega$ contains the geometric size of the control volumes. This discretization does not produce artificial diffusion and convectively preserves the energy of the flow [15,33]. The discrete gradient operator and the divergence operator are each other's negative transpose, i.e. $\mathsf{G} = -\mathsf{M}_0^T$ mimicking the analytic symmetry $\nabla = -(\nabla\cdot)^T$, such that the work done by the pressure vanishes discretely.

Imposing discrete mass conservation (2) at the new time level, substitution of (3) results in a discrete Poisson equation for the pressure:

$$\delta t\,\mathsf{M}_0\Omega^{-1}\mathsf{G}\mathsf{p}^{n+1} = \mathsf{M}_0\tilde{\mathbf{u}} + \mathsf{M}_\Gamma\mathbf{u}_\Gamma^{n+1}. \tag{4}$$

3

Here $\Gamma$ is the boundary of the fluid domain where boundary conditions involving the velocity are prescribed; it includes the fluid-solid interface $\Gamma_{\mathrm{FS}}$.

For future reference, the fluid dynamic problem will be formally abbreviated as

$$\mathsf{M}_{\mathrm{ad}}\ddot{\mathbf{d}}_{\Gamma_{\mathrm{FS}}} = -\mathbf{f}_{\Gamma_{\mathrm{FS}}}. \tag{5}$$

Here, $\mathsf{M}_{\mathrm{ad}}$ is the so-called fluid added-mass operator, which governs the relation between the motion of an immersed body and the reactive forces excerted by the fluid. Further, $\mathbf{d}$ is the displacement of the fluid-solid interface.

## 2.2 Structural model

For simplicity in this study, the structure is selected to be a one dimensional Euler–Bernoulli beam. Assuming a constant cross section $A = TW$ for the beam (thickness $T$ and width $W$), its equation of motion is

$$\rho_s A \frac{\partial^2 d}{\partial t^2} + EI \frac{\partial^4 d}{\partial s^4} = f, \tag{6}$$

with appropriate initial and boundary conditions. Here, $s$ denotes a coordinate along the beam, $d$ the beam deformation, $\rho_s$ the beam density, $E$ Young's modulus, $I$ the second moment of inertia and $f$ the load per unit length of the beam.

The structural response is modeled with a finite element method. Omitting the technical details, the resulting discrete set of equations can be written in the form

$$\mathsf{M}_{\mathrm{eb}}\ddot{\mathbf{d}} + \mathsf{K}_{\mathrm{eb}}\mathbf{d} = \mathbf{f}_{\Gamma_{\mathrm{FS}}}, \tag{7}$$

where $\mathsf{M}_{\mathrm{eb}}$ is the discrete mass operator and $\mathsf{K}_{\mathrm{eb}}$ the discrete stiffness operator. The temporal integration of the structure equations is performed by means of the generalized-$\alpha$ method [34].

## 2.3 Fluid-solid coupling conditions

The coupling relations along the fluid-solid interface $\Gamma_{\mathrm{FS}}$ consist of two relations. The kinematic condition states that the motion of the interface on both sides matches, whereas the dynamic condition ensures equilibrium of stresses:

$$\text{kinematic} \quad \mathbf{u} = \frac{\partial \boldsymbol{d}}{\partial t}\mathbf{n} \; ; \qquad \text{dynamic} \quad \overline{\overline{\sigma}}_f \cdot \mathbf{n} = \overline{\overline{\sigma}}_s \cdot \mathbf{n}. \tag{8}$$

## 3 NUMERICAL COUPLING METHODS

### 3.1 Numerical coupling with a solid body

Traditional weak (hierarchical) coupling methods, with information exchange once per time step, are only numerically stable within a restricted range of added-mass ratios. If the application covers a larger range, one has to resort to strong (simultaneous) coupling [35]. Usually, some form of subcycling within each time step is applied, where information is exchanged at the 'hearts' of the numerical algorithms (like in a monolithic code). For two-way coupled problems, a monolithic procedure of the subdomains would be most powerful. However, such a simultaneous approach is not always possible, e.g. when 'black-box' commercial codes are being used, as the

4

subdomain solvers have to be coupled at a deep iterative level. In this section we will describe an approach that tries to combine the simplicity of a hierarchical coupling approach with the iterative power of a monolithic approach.

**Segregated coupling**   The stability of the two-way coupled system can be investigated in an abstract setting. On both sides of the fluid-body interface $\Gamma_{FS}$ physical properties need to be continuous, as expressed in the kinematic and dynamic conditions (8). Thus the coupling problem can be formulated in terms of interface variables only: the velocity along the interface $\mathbf{u}_\Gamma$ and the local or total load exerted by the fluid to the structure $\mathbf{f}_\Gamma$ (for an elastic body found from the local stresses, for a solid body found from their integration along the interface).

   The solid body reacts by accelerating due to the exerted force from the fluid. For a solid body a six degrees of freedom (DOF) mass operator ($\mathsf{M}_{\mathrm{sb}}$) containing inertial properties of the body rules its dynamic response. The fluid, on the other hand, reacts to the accelerated solid body with a new pressure field. The so-called added-mass operator ($\mathsf{M}_{\mathrm{ad}}$) describes the fluid's response. Thus we can formulate the coupled problem in abstract notation as

$$\text{solid body dynamics}\quad \mathsf{M}_{\mathrm{sb}}\ddot{\mathbf{d}}_\Gamma^{k+1} = \mathbf{f}_\Gamma^k \; ; \quad \text{fluid dynamics}\quad \mathbf{f}_\Gamma^{k+1} = -\mathsf{M}_{\mathrm{ad}}\ddot{\mathbf{d}}_\Gamma^{k+1}. \qquad (9)$$

We have already indicated the usual iterative process which is used to solve this set of, basically, 2 equations in 2 unknowns. Its formal amplification operator follows as

$$\mathbf{f}_\Gamma^{k+1} = -\mathsf{M}_{\mathrm{ad}}\mathsf{M}_{\mathrm{sb}}^{-1}\mathbf{f}_\Gamma^k, \text{ which is stable if and only if } \rho(\mathsf{M}_{\mathrm{ad}}\mathsf{M}_{\mathrm{sb}}^{-1}) < 1. \qquad (10)$$

In other terms, the ratio of the added mass to the solid body mass for each DOF, more precisely all eigenvalues, should be less than one. If the problem violates this requirement, methods like the under-relaxation method, can only keep this value below unity at the cost of (severely) increasing computational effort.
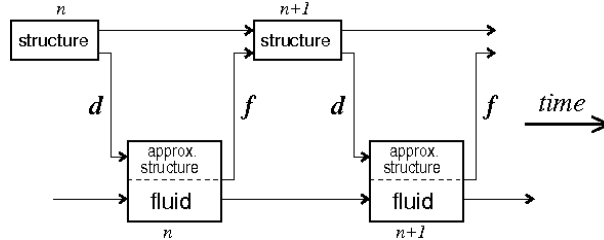


**Figure 2**: Coupling strategy for simulaing the interaction between a solid-body/structure and a fluid. To improve the numerical stability, an interaction law is used consisting of an approximate model for the solid-body/structure dynamics.

**Quasi-simultaneous coupling**   It is not necessary to perform a *fully* simultaneous coupling. A good approximation of one of the two submodels is sufficient to be fully intertwined with the other submodel. The difference between the approximation and the original submodel can be dealt with in the traditional, weak fashion. Such a coupling is called *quasi-simultaneous*, and

5

was introduced in a steady, aerodynamic context in the late 1970s [36, 37]. Recently, the method has been re-discovered in the FSI community [11, 38].

In time-integration terms, the bulk of the interaction is treated implicitly, the remaining part explicitly. Numerical stability of this approach requires that, roughly spoken, the implicit part contains at least 'half of the physics', which is a very weak requirement. An essential step is that the equations approximating the other submodel, such as an elastic wall model, are considered boundary conditions for the fluid flow equations. In particular, they will show up as a boundary condition in the pressure Poisson equation.

In this quasi-simultaneous method an approximation of the body dynamics is solved simultaneously with the fluid. This *interaction law* anticipates the body response in advance of the actual solid dynamics computation. As such, the interaction law is an approximation $\widetilde{\mathsf{M}_{sb}^{-1}}$ to the inverse mass operator $\mathsf{M}_{sb}^{-1}$ of the solid body dynamics (9a). In the iterative process within each time step, the interaction law is exploited as

$$\text{solid body} \qquad\qquad \ddot{\mathbf{d}}_\Gamma^{k+1} = \mathsf{M}_{sb}^{-1}\mathbf{f}_\Gamma^k, \qquad\qquad (11)$$

$$\text{interaction law} \qquad\qquad \dot{\mathbf{u}}_\Gamma - \widetilde{\mathsf{M}_{sb}^{-1}}\mathbf{f}_\Gamma^{k+1} = \ddot{\mathbf{d}}_\Gamma^{k+1} - \widetilde{\mathsf{M}_{sb}^{-1}}\mathbf{f}_\Gamma^k, \qquad\qquad (12)$$

$$\text{fluid} \qquad\qquad \mathbf{f}_\Gamma^{k+1} + \mathsf{M}_{ad}\dot{\mathbf{u}}_\Gamma = 0. \qquad\qquad (13)$$

Eliminating $\ddot{\mathbf{u}}_\Gamma$ leads to the following iterative process, which can be compared to (10):

$$\left(\mathsf{I} + \mathsf{M}_{ad}\widetilde{\mathsf{M}_{sb}^{-1}}\right)\mathbf{f}_\Gamma^{k+1} = -\mathsf{M}_{ad}\left(\mathsf{M}_{sb}^{-1} - \widetilde{\mathsf{M}_{sb}^{-1}}\right)\mathbf{f}_\Gamma^k, \qquad\qquad (14)$$

where $\mathsf{I}$ is the unit operator. In mathematical terms, the interaction law should neutralize the most cumbersome eigenvalues of the iteration matrix.

This relation simplifies to (10) if the interaction law is zero, or in other words not employed, which breaks down if $\mathsf{M}_{ad}$ is large. Similar to the segregated method, the iterative procedure is stable if and only if the spectral radius of the amplification matrix is less than one, i.e. $\rho((\mathsf{M}_{ad}^{-1} + \widetilde{\mathsf{M}_{sb}^{-1}})^{-1}(\mathsf{M}_{sb}^{-1} - \widetilde{\mathsf{M}_{sb}^{-1}})) < 1$. When $(\widetilde{\mathsf{M}_{sb}^{-1}} - \mathsf{M}_{sb}^{-1})$ is sufficiently small, this process will converge, in spite of a possibly large $\mathsf{M}_{ad}$.

## 3.2 Numerical coupling with an elastic body

Because the structural equation (7) contains both $\ddot{\mathbf{d}}$ and $\mathbf{d}$, first a discrete time integration is carried out. Thereafter, an analysis similar to the above can be carried out. Then the discrete version of the hierarchically coupled problem at the new time level can be denoted as

$$\text{elastic body} \qquad\qquad \left(\frac{\mathsf{M}_{eb}}{\delta t^2} + \mathsf{K}_{eb}\right)\mathbf{d}_\Gamma^{k+1} = \mathbf{f}_\Gamma^k + \dots, \qquad\qquad (15)$$

$$\text{fluid} \qquad\qquad \mathbf{f}_\Gamma^{k+1} = -\frac{\mathsf{M}_{ad}}{\delta t^2}\mathbf{d}_\Gamma^{k+1}. \qquad\qquad (16)$$

Here, $\mathsf{M}_{eb}$ denotes the discrete elastic body mass operator, while $\mathsf{K}_{eb}$ is the discrete elastic body stiffness operator; compare (7). The contributon from the previous time steps is omitted in view of clarity; it is just an inhomogeneous term in the right-hand side, which is not relevant for the convergence of the subiterations per time step.

6

Matrices $\mathsf{M}_{\mathrm{eb}}$ and $\mathsf{K}_{\mathrm{eb}}$ can be simultaneously diagonalized as $\mathsf{Q}^T\mathsf{M}_{\mathrm{eb}}\mathsf{Q} = \mathsf{I}$ and $\mathsf{Q}^T\mathsf{K}_{\mathrm{eb}}\mathsf{Q} = \Lambda$, where $\mathsf{Q}$ contains the normalized elastic body eigenvectors with eigenvalues $\Lambda$. In this way, the elastic body dynamics (15) can be rewritten as

$$\text{elastic body} \qquad \mathsf{Q}^{-T}\left(\frac{\mathsf{I}}{\delta t^2} + \Lambda\right)\mathsf{Q}^{-1}\mathbf{d}_\Gamma^{k+1} = \mathbf{f}_\Gamma^k. \qquad (17)$$

The displacement $\mathbf{d}^{k+1}$ can be eliminated from the system of equations (16) and (17), after which the iterative process can be written as

$$\mathbf{f}^{k+1} = -\mathsf{M}_{\mathrm{ad}}\mathsf{Q}(\mathsf{I} + \delta t^2\Lambda)^{-1}\mathsf{Q}^T\mathbf{f}^k. \qquad (18)$$

For small enough $\delta t$, the amplification factor simplifies to $\mathsf{M}_{\mathrm{ad}}\mathsf{Q}\mathsf{Q}^T$. For a solid body with 6 DOF, $\mathsf{Q}\mathsf{Q}^T$ can be replaced by the inverse solid-body mass $\mathsf{M}_{\mathrm{sb}}^{-1}$.

It can be shown [39] that the lower modes are most delicate, as they correspond with the largest fluid added mass. Therefore we take care that these modes are treated more simultaneous. Thus we construct an approximation of the full elastic equations, built from the lowest elastic modes of the structure.

## 4  EXAMPLES

### 4.1  Tank with membrane bottom

In order to assess the performance of the quasi-simultaneous approach for different mass ratios, a test case has been designed in which this ratio can be varied. Also, the physical contents of the interaction law has been varied.
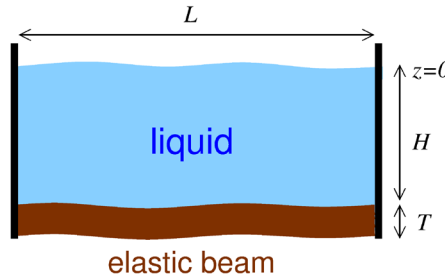


**Figure 3**: Schematic of the first test case; the domain with free-surface flow on top and flexible beam at the bottom.

At the bottom of a rectangular container ($1.0 \times 0.1 \times 0.5\,\mathrm{m}^3$) filled with 50 kg of water, a flexible beam is placed, as illustrated in Fig. 3. The mass of the beam is varied between 1 kg and 50 kg; its module of elasticity is 1 MPa. The interaction law is made out of truncated structural modes; the number of modes dictates its accuracy.

Cases with mass ratio 1 and 50 are presented, where the number of included modes is increased in order of relevance. Figure 4 shows the convergence history during the first time step. The effect of the number of modes in the interaction law can be inferred. For a small added-mass ratio one mode suffices, but for the more difficult mass ratio 50 it is profitable to include more modes in the interaction law. This behaviour is perfectly in line with the theoretical stability analysis in [39].
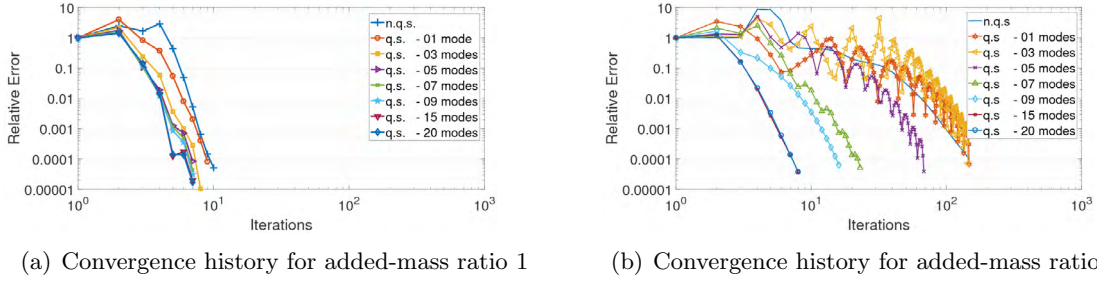
7

(a) Convergence history for added-mass ratio 1     (b) Convergence history for added-mass ratio 50

**Figure 4**: Convergence history of the quasi-simultaneous method for the first time step for an increasing number of included modes.

## 4.2 Free-fall life boat

The second example concerns a simulation of a free-fall life boat (Fig. 1). During the penetration of the free water surface the added mass can become quite large with added-mass ratios upto 40. Hence it is a perfect test case to evaluate the performance of the quasi-simultaneous coupling method. The main finding is summarized in Fig. 5(right). It shows the amount of floating-point operations to solve the pressure Poisson equation including the FSI-iterations that are required per time step to converge the coupling with the moving solid body. In particular, the dependence of this computational effort with the added-mass ratio is shown. The graph shows that at larger added-mass ratios the quasi-simultaneous coupling method is much more efficient than the 'classical' segregated coupling; it is even more efficient at small added-mass ratios.



**Figure 5**: Free-fall life boat being launched (left). The computational effort required per time step for the FSI coupling (right).

## 4.3 CALM buoy

The third case is a validation against model tests of a CALM buoy (Fig. 6) in a shallow water basin at MARIN [40]. These tests include the freely decaying motion of the buoy after being released from a given position into calm water. This allows us to compare the simulated and measured natural periods as well as the amount of hydrodynamic damping. The buoy in its default configuration has been modelled as a cylinder with a diameter of 12 m and a height of 6.5 m.

The simulation has been performed at different grids, with approximately 6, 10 and 18 cells
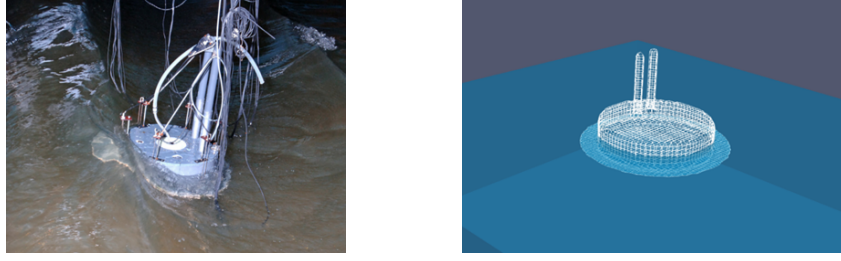
8

**Figure 6**: Model of the CALM buoy in the shallow water basin at MARIN (left) and the geometrical representation in the simulations (right).

per cylinder diameter. The results for heave motion are shown in Fig. 7. Using the approach of Eca et al. [41], the numerical uncertainty has been assessed from these three grids and is also indicated. The resulting uncertainty was found quite small, whereas it is understandable that for later times in the simulation the uncertainty increases. The validation of the simulations was monitored by a comparison with the experiments at MARIN and also indicated in Fig. 7. The period as well as damping of the heave motion are found well-predicted.
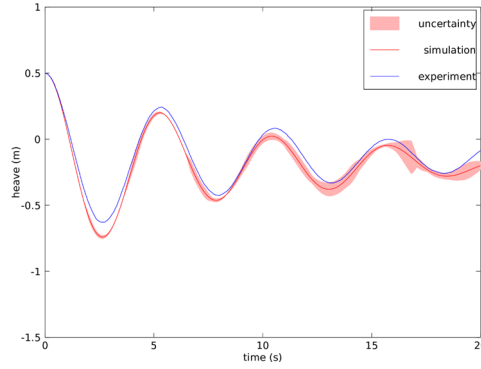


**Figure 7**: Heave motions of a free-floating CALM buoy in simulation and experiment.

## 5 ABSORBING BOUNDARY CONDITIONS

In the CALM-buoy simulations, the computational domain has to be restricted to a finite region; one has to take care that no numerical reflections from these artificial domain boundaries enter the physical region of interest. To minimize these reflections a new type of absorbing boundary conditions (ABC) has been developed, which can adapt itself to the passing waves [21, 42]. Also, the effect of current (in arbitrary direction) has been included. In 2D, Peregrine [43] already studied the effect of current on the dispersion relation. In 3D the dispersion relation involving current $\mathbf{U}$ reads, using the abbreviation $k = |\mathbf{k}|$,

$$\omega_{\pm} = \frac{\mathbf{U} \cdot \mathbf{k}}{k} + c_{k0} \quad \text{with} \quad c_{k0} = \sqrt{gh}\sqrt{\frac{\tanh(kh)}{kh}}. \tag{19}$$

9

The ABC is basically of Sommerfeld type, which in 3D reads as

$$\left[ \cos \alpha \left( \frac{\partial}{\partial t} + \mathbf{U} \cdot \nabla \right) + c_{k0} \frac{\partial}{\partial n} \right] \phi_w = 0, \tag{20}$$

where $\alpha$ is the angle between the wave $\mathbf{k}$ and the normal $\mathbf{n}$. This new condition lets waves with wave number $\mathbf{k}$ pass freely; it is not unique. Further, $\phi_w$ is the wave component of the potential, which is reformulated in terms of pressure $p$ and velocity $\mathbf{u}$, using the unsteady Bernoulli equation. This results in a relation between $p$ and $\mathbf{u}$ which is used as a boundary condition to the pressure Poisson equation, similar to the interaction law for fluid-structure interaction that we discussed above. The phase speed $c_{k0}$ is replaced by a Padé approximation, with the unknown wave number $\mathbf{k}$ found from the local solution [21, 42].

Figure 8 shows a simulation of an oscillating sphere, with prescribed motion, which generates outgoing waves. A current is present, running in diagonal direction through the domain. The current makes the radiating circles no longer concentric. The domain has been kept rather small, in order to study reflections at the boundaries. The figure clearly shows no visible irregularities near the domain boundaries, demonstrating the potential of the new ABC.
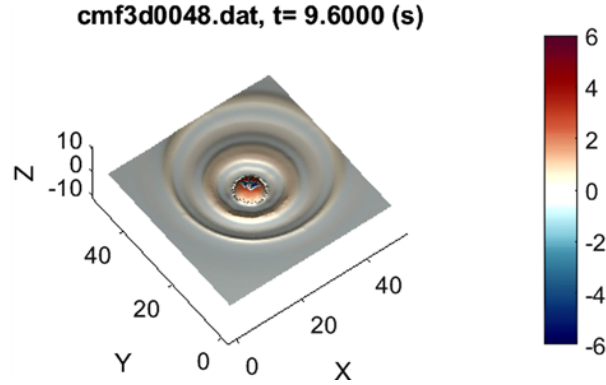


**Figure 8**: Oscillating buoy in a current, generating non-concentric waves. Observe the regularity of the results at the boundary of the computational domain.

## 6 CONCLUSION

Several of the newly-developed ingredients of the ComFLOW simulation method have been sketched. Firstly, a quasi-simultaneous numerical coupling method has been presented. It can handle large added-mass ratios efficiently and can also be extended to cover the coupling with elastically-deforming objects. The lower elastic modes are found the most 'tricky' and can be 'tamed' by including them in the interaction law. Secondly, ComFLOW's absorbing boundary condition which adjusts itself to the oncoming waves has been extended to cover the influence of current. Several examples of verification and validation have been included.

10

# REFERENCES

[1] S. Haver. Evidences of the existence of freak waves. In Ifremer, editor, *Rogue Waves 2000, Proc. of Int. Workshop*, pages 129–140, Brest (France), 29-30 November, 2000.

[2] O. M. Faltinsen. *Sea Loads on Ships and Offshore Structures*. Cambridge University Press, 1999.

[3] B. Buchner. *Green water on ship-type offshore structures*. PhD Thesis, University of Delft, Delft, The Netherlands, November 2002.

[4] B. Molin and J. Ferziger. Hydrodynamique des structures offshore. *Appl. Mech. Rev.*, 56:B29, 2003.

[5] W. Tsai and D. K. P. Yue. Computation of nonlinear free-surface flows. *Ann. Rev. Fluid Mech.*, 28:249–278, 1996.

[6] C. W. Hirt and B. D. Nichols. Volume of fluid (VOF) method for the dynamics of free boundaries. *J. Comput. Phys.*, 39:201–25, 1981.

[7] W. J. Rider and D. B. Kothe. Reconstructing volume tracking. *J. Comput. Phys.*, 141:112–152, 1998.

[8] T. Yabe, F. Xiao, and T. Utsumi. The constrained interpolation profile method for multiphase analysis. *J. Comput. Phys.*, 169:556–593, 2001.

[9] S. J. Osher and G. Tryggvason (eds.). Special issue on 'Computational Methods for Multiphase Flows'. *J. Comput. Phys.*, 169:249–759, 2001.

[10] Mathieu Durand, Alban Leroyer, Corentin Lothodé, Frédéric Hauville, Michel Visonneau, Ronan Floch, and Laurent Guillaume. Fsi investigation on stability of downwind sails with an automatic dynamic trimming. *Ocean Engineering*, 90:129–139, 2014.

[11] David Gross. New quasi-monolithic method to solve dynamic fluid-structure interaction problems on membranes. In *Textiles composites and inflatable structures VII: proc. VII Int. Conf. on Textile Composites and Inflatable Structures, Barcelona, Spain. 19-21 October, 2015*, pages 344–355. CIMNE, 2015.

[12] Daniel Oliveira, Aldina Santiago, and Constança Rigueiro. Fluid structure interaction in offshore environment. In J.F. Silva Gomes and S.A. Meguid, editors, *Proc. 5th Int. Conf. on Integrity-Reliability-Failure*, Porto (Portugal), July 24-28 2016. Paper ref: 6258.

[13] R. Verstappen. When does eddy viscosity damp subfilter scales sufficiently? *J. Sci. Comput.*, 49(1):94–110, 2011.

[14] W. Rozema. *Low-dissipation methods and models for the simulation of turbulent subsonic flow*. PhD thesis, University of Groningen, 2015.

[15] Wybe Rozema, Roel W. C. P. Verstappen, Johan C. Kok, and Arthur E. P. Veldman. Low-dissipation simulation methods and models for turbulent subsonic flow. *Arch. Comput. Meth. Eng.*, 2019. DOI: 10.1007/s11831-018-09307-7.

[16] Mahdi Abkar, Hyun J. Bae, and Parviz Moin. Minimum-dissipation scalar transport model for large-eddy simulation of turbulent flows. *Physical Review Fluids*, 1(4):041701, 2016.

[17] A. E. P. Veldman, R. Luppes, P. van der Plas, H. J. L. van der Heiden, J. Helder, and T. Bunnik. Turbulence modeling for locally-refined free-surface flow simulations in offshore applications. In *Proc. Int. Symp. Offshore Polar Eng. ISOPE2015*, Kona (Hawaii, USA), 23-27 June 2015. paper ISOPE2015-TPC-0282.

[18] H.J.L. van der Heiden. *Modelling viscous effects in offshore flow problems - a numerical study*. PhD thesis, University of Groningen, 2019.

[19] K. M. T. Kleefsman, G. Fekken, A. E. P. Veldman, B. Iwanowski, and B. Buchner. A Volume-of-Fluid based simulation method for wave impact problems. *J. Comput. Phys.*, 206:363–393, 2005.

[20] D. L. Youngs. An interface tracking method for a 3d Eulerian hydrodynamics code. Technical Report AWRE/44/92/35, Atomic Weapons Research Establishment, 1987.

[21] B. Düz. *Wave generation, propagation and absorption in CFD simulations of free surface flows*. PhD thesis, Technical University Delft, 2015.

[22] J. Gerrits. *Dynamics of Liquid-Filled Spacecraft*. PhD thesis, University of Groningen, The Netherlands, 2001.

11

[23] G. Fekken. *Numerical simulation of free-surface flow with moving objects*. PhD Thesis, University of Gronin-gen, The Netherlands, 2004.

[24] K. M. T. Kleefsman. *Water impact loading on offshore structures - a numerical study*. PhD thesis, University of Groningen, The Netherlands, 2005.

[25] R. Wemmenhove. *Numerical simulation of two-phase flow in offshore environments*. PhD Thesis, University of Groningen, The Netherlands, 2008.

[26] P. R. Wellens. *Wave simulation in truncated domains for offshore applications*. PhD Thesis, Technical University Delft, The Netherlands, 2012.

[27] P. van der Plas. *Local grid refinement for free-surface flow simulations*. PhD thesis, University of Groningen, 2017.

[28] M. Dröge and R. Verstappen. A new symmetry-preserving Cartesian-grid method for computing flow past arbitrarily shaped objects. *Int. J. Numer. Meth. Fluids*, 47:979–985, 2005.

[29] Y. Cheny and O. Botella. The LS-STAG method; a new immersed boundary/level-set method for the computation of incompressible viscous flows in complex moving geometries with good conservation properties. *J. Comput. Phys.*, 229:1043–1076, 2010.

[30] H. B. Gu, D. M. Causon, C. G. Mingham, and L. Qian. Development of a free surfcae flow solver for the simulation of wave/body interactions. *Eur. J. Mech. B/Fluids*, 38:1–17, 2013.

[31] A. E. P. Veldman, P. van der Plas, H. Seubers, J. Helder, and K.-W. Lam. Adaptive grid refinement for two-phase offshore applications. In *Proc. 37th Int. Conf. Ocean, Offshore Arctic Eng. OMAE2018*, Madrid (Spain), 17-22 June 2018. paper OMAE2018-77309.

[32] F. H. Harlow and J. E. Welch. Numerical calculation of time-dependent viscous incompressible flow of fluid with free surface. *Phys. Fluids*, 8:2182–2189, 1965.

[33] R. W. C. P. Verstappen and A. E. P. Veldman. Symmetry-preserving discretization of turbulent flow. *J. Comput. Phys.*, 187:343–368, 2003.

[34] J. Chung and G. M. Hulbert. A time integration algorithm for structural dynamics with improved numerical dissipation: the generalized-$\alpha$ method. *J. Appl. Mech.*, 60(2):371–375, August 1992.

[35] P. Causin, J. F. Gerbau, and F. Nobile. Added-mass effect in the design of partitioned algorithms for fluid-structure problems. *Comput. Methods Appl. Mech. Engr.*, 194:4506–4527, 2005.

[36] A. E. P. Veldman. New, quasi-simultaneous method to calculate interacting boundary layers. *AIAA J.*, 19:79–85, 1981.

[37] A. E. P. Veldman. A simple interaction law for viscous-inviscid interaction. *J. Eng. Math.*, 65:367–383, 2009.

[38] Mathieu Durand. *Interaction fluide-structure souple et l egere, application aux voiliers*. PhD thesis, Ecole Centrale de Nantes (ECN), 2012.

[39] Arthur E. P. Veldman, Peter van der Plas, Henk Seubers, Matin Hosseini Zahraei, Xing Chang, Peter R. Wellens, and Joop Helder. Overview of fluid-structure coupling in ansys-cfx. In *Proc. 38th Int. Conf. Offshore Mech. Arctic Eng.*, pages OMAE2019–96321, Glasgow (Scotland), June 9-14 2019.

[40] T. H. J. Bunnik and A. G. van Doeveren. CALM buoy model tests. Technical Report report 18378-3-BT, MARIN, 2008.

[41] Luis Eça and Martin Hoekstra. Discretization uncertainty estimation based on a least squares version of the grid convergence index. In *Proc. 2nd Workshop on CFD Uncertainty Analysis, Instituto Superior Tecnico, Lisbon*, 2006.

[42] B. Düz, M. J. A. Borsboom, P. R. Wellens, A. E. P. Veldman, and R. H. M. Huijsmans. An absorbing boundary condition for free-surface water waves. *Comput. Fluids*, 156:562–578, 2017.

[43] D. H. Peregrine. Interaction of water waves and currents. *Advances in Applied Mechanics.*, 16:9–117, 1976.

12